JOURNAL OF AIRCRAFT
Vol. 31, No. 1, Jan.–Feb. 1994

Frequency-Domain Analysis of Fluctuating Pressure on a Pusher Propeller Blade Surface

Saeed Farokhi,* Ray Taghavi,† and Kyle K. Wetzel‡
University of Kansas, Lawrence, Kansas 66045

Chordwise distribution of unsteady surface pressure is measured on a pylon-mounted pusher propeller in flight. Spectral decomposition of the fluctuating surface pressure signals reveals a strong presence of upstream wake interaction. The growth and decay behavior of the fundamental disturbance wave along the propeller chord exhibits the same characteristics as a separated, reattaching shear layer. Frequency-domain analysis further suggests a single or multiple vortex-shedding phenomenon from the pusher propeller trailing edge, per revolution, in an upstream wake interaction. The rms amplitude of higher harmonics (i.e., k = 3, 4, 5, and 6) along the propeller chord attains values corresponding to boundary-layer random turbulence levels. Joint statistical properties between selected transducers on the propeller suction surface suggest a linear frequency response of the dynamical system to the fundamental and first harmonic disturbances, while higher-frequency Fourier components result in a nonlinear response behavior.

Nomenclature

A_k = complex Fourier coefficient
A_k^* = complex conjugate of A_k
C_{P_k} = unsteady surface pressure coefficient for the kth harmonic
C_{p_1} = unsteady surface pressure coefficient for the fundamental wave
c = propeller chord length, m
D = propeller diameter, 2.54 m
E = expected value, ensemble average
f = propeller shaft frequency
$G_{\xi\eta}(f)$ = cross spectral density function
$G_{\xi\xi}(f)$, $G_{\eta\eta}(f)$ = power spectral density function
J = propeller advance ratio, V/fD
k = harmonics of shaft rotation frequency
M = number of revolutions used in statistical data analysis, 700
M_r = helical Mach number
M_∞ = flight Mach number
m = revolution index
N = number of data points per revolution, 330
n = data point index
P_∞ = flight static pressure, Pa
$(p_k)_{\text{rms}}$ = rms pressure of the kth harmonic of shaft rotation
$(p_1)_{\text{rms}}$ = rms amplitude of the fluctuating pressure for fundamental harmonic (Pa); i.e., shaft order 1
R = propeller radius, 1.27 m
T = propeller period of revolution, s
t = time
V = flight speed, m/s
x = coordinate along propeller chord, m
β_{prop} = propeller pitch angle measured with respect to plane of rotation
β_{75R} = helical flow angle at 0.75 radius measured with respect to propeller plane of rotation
β_{90R} = same as β_{75R}, but at 90% propeller radius
γ = ratio of specific heats for air, 1.4
$\gamma^2_{\xi,\eta}(f)$ = coherence function
$\Delta\beta$ = $\beta_{\text{prop}} - \beta_{75R}$ or $\beta_{\text{prop}} - \beta_{90R}$
Δt = time interval between data points in one revolution, s
$\eta_T(f)$ = finite Fourier transform of $\eta(t)$
$\xi_T(f)$, $\xi^*_T(f)$ = finite Fourier transform of $\xi(t)$ and its complex conjugate
$\xi(t)$, $\eta(t)$ = blade-mounted transducer pressure-time history at two chordwise locations
ω = propeller shaft rotational speed, rpm

Introduction

IN developing unsteady aerodynamic loading models and predicted noise spectra of a pusher propeller, miniature, high-frequency, blade-mounted transducers (BMTs) can provide valuable and direct information. The fluctuating propeller surface pressure response to incoming flow nonuniformities (e.g., due to pylon or wing wake) is recorded over many propeller revolutions, e.g., 700. Statistical analysis of the data provides the basis for better physical understanding of the unsteady flow phenomena on a pusher propeller operating in the transonic regime. The data are particularly useful if many pressure transducers are involved in a chordwise distribution and at least two radii along the propeller blade. This primarily stems from the three-dimensional nature of the propeller boundary layer and tip compressibility effects. To simulate, in a wind tunnel, the environment in which a pusher propeller is exposed to realistic flight conditions is nearly impossible. For this reason, a propeller-driven test-bed aircraft of pusher configuration is flight tested with an instrumented propeller blade. A total of 22 BMTs were distributed at the 75 and 90% propeller radii. The pressure-time history of these BMT signals revealed peculiar and intriguing blade surface phenomena, which are discussed by Farokhi.[1] In particular, a new type of periodic disturbance of long-time scale, compared to propeller period of revolution, was discovered at positions beyond 60% chord on the suction surface in the transonic regime.[1,2]

Received Feb. 18, 1992; revision received Oct. 12, 1992; accepted for publication Oct. 25, 1992.

*Professor of Aerospace Engineering and Director of the Flight Research Laboratory, Center for Research, Inc. Senior Member AIAA.
†Assistant Professor of Aerospace Engineering. Member AIAA.
‡Undergraduate Research Assistant, Flight Research Laboratory, Center for Research, Inc.; currently Graduate Fellow at the University of Illinois, Urbana, IL. Member AIAA.

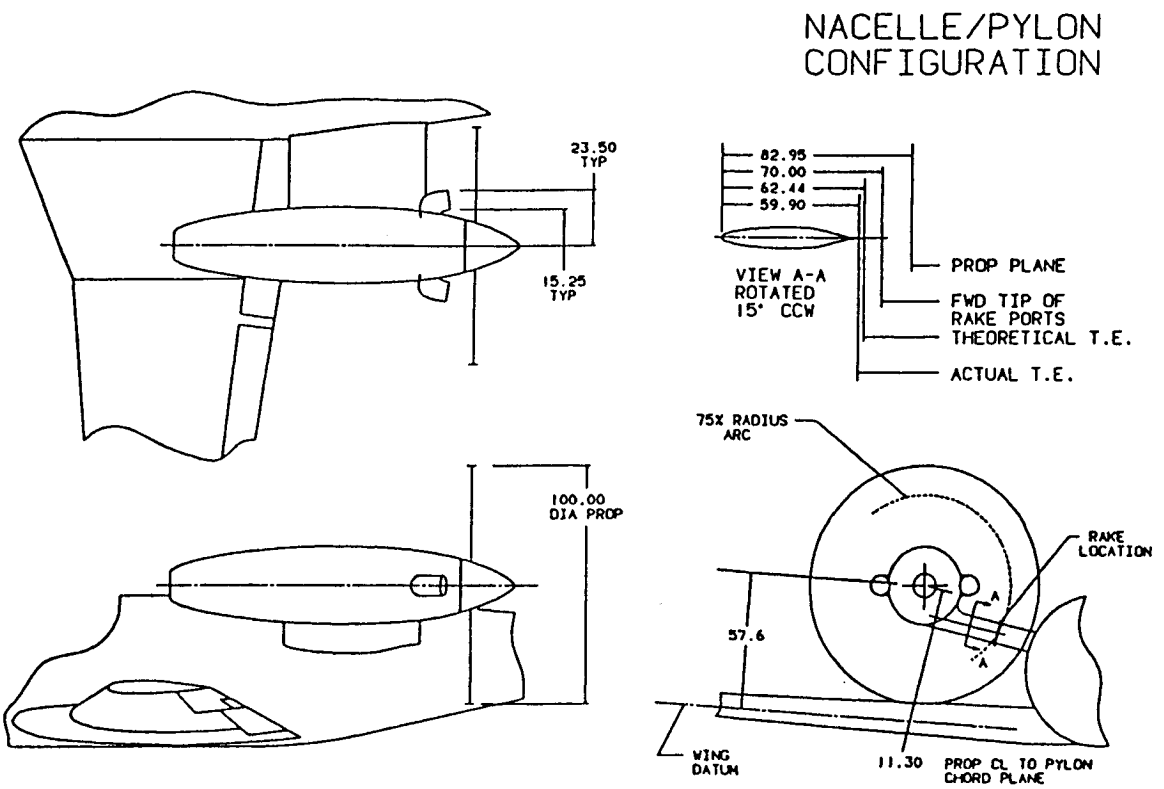

Fig. 1 Flight configuration of the advanced turboprop test-bed aircraft.

Heidelberg and Clark[3] examined unsteady blade surface response to periodic angle of attack on an advanced, highly swept, (single rotation) SR-3 propeller in a wind tunnel. A distribution of seven blade-mounted pressure transducers at two radii and on two blades revealed a cascading effect for the eight-bladed version of SR-3 propeller tests. The appearance of shocks on the suction surface was identified by the authors as a prime candidate for nonsinusoidal pressure response near the propeller leading edge (i.e., 0.1-chord BMT position). Due to the very limited number of pressure transducers in the chord and spanwise direction used in the wind-tunnel test of SR-3 propeller, the growth and decay of the fundamental harmonic wave (i.e., shaft order 1) could not be deduced from Heidelberg and Clark's tests.[3] Furthermore, as the propeller in Ref. 3 was of tractor configuration, no inflow distortion (as in upstream wake interaction) was simulated. The acoustic study of the SR-3 propeller at two angles of attack was conducted by Ditmar and Jeracki[4] at NASA Lewis. Other blade surface pressure measurements were obtained in the past on the fan blades of a turbofan engine.[5,6] The BMTs on the fan blades registered a one-cycle pressure wave, which is believed to be due to flow angularity at the compressor face. This implies that the fan plane of rotation is not, in practice, perfectly normal to the incoming stream—which essentially rules out the scenario of axisymmetric flow often assumed for rotating machinery. Besides the angle of attack which is the dominant source of propeller cyclic loading, actual flight environment involves sideslip which compounds the flow angularity at the propeller (or compressor) face. The counterpart of in-flight sideslip is the crosswind problem for takeoff and landing phase of an aircraft propulsion system.

Spectral analysis of a periodically unsteady flowfield, as in the upstream wake-pusher propeller interaction problem, where the analyzed frequencies center on the periodic events, in principle, sorts out the phase-locked coherent features from an otherwise random unsteadiness in the flowfield. Farokhi's recent work[1] is extended into the frequency domain in this article. Chordwise evolutions of unsteady pressure coefficient for the fundamental and higher harmonics (centered on shaft angular frequency) at two radii and various flight conditions (i.e., propeller loading conditions) are presented. The initial growth and subsequent decay of the fundamental disturbance on the propeller suction surface exhibit the same characteristics as a separated reattaching shear layer. This behavior is interpreted as the leading-edge vortex roll-up and separation. Furthermore, unsteady vortex shedding at the trailing edge imposes a distinct footprint on the $(P_1)_{\text{rms}}$ wave beyond x/c of 0.85. This phenomenon is repeatedly observed in the chordwise evolution of the fundamental harmonic. This interpretation of the large-scale, coherent trailing-edge events (or footprints on the propeller trailing edge) as vortex shedding is consistent with the classical unsteady aerodynamic theory. Pusher propeller interaction with the pylon wake resulting in multiple vortex sheddings from the trailing edge is a new result and is further discussed in this article. Flight configuration of the advanced turboprop testbed aircraft is shown in Fig. 1. For details on engine installation, instrumentation, and pylon wake profiles, the reader may consult Refs. 1 and 2.

Frequency-Domain Analysis of Unsteady Pressure

BMT signals over M revolutions are sampled N times per revolution with equal time-spacing Δt. An average waveform is then constructed by using the formula

$$\bar{P}_n = \frac{1}{M}\sum_{m=1}^{M} P_{m,n} \tag{1}$$

where m and n are the corresponding mth revolution and the nth data point in that revolution, respectively. Due to ergodicity of the random process involved, the average pressure-time history obtained from Eq. (1) is Fourier transformed into frequency domain. The frequencies chosen for the spectral analysis center on the harmonics of shaft rotation frequency. The rms of the kth harmonic $(P_k)_{\text{rms}}$ is calculated from

$$(P_k)_{\text{rms}} = [|A_k A_k^* - P_0^2|]^{1/2} \tag{2}$$

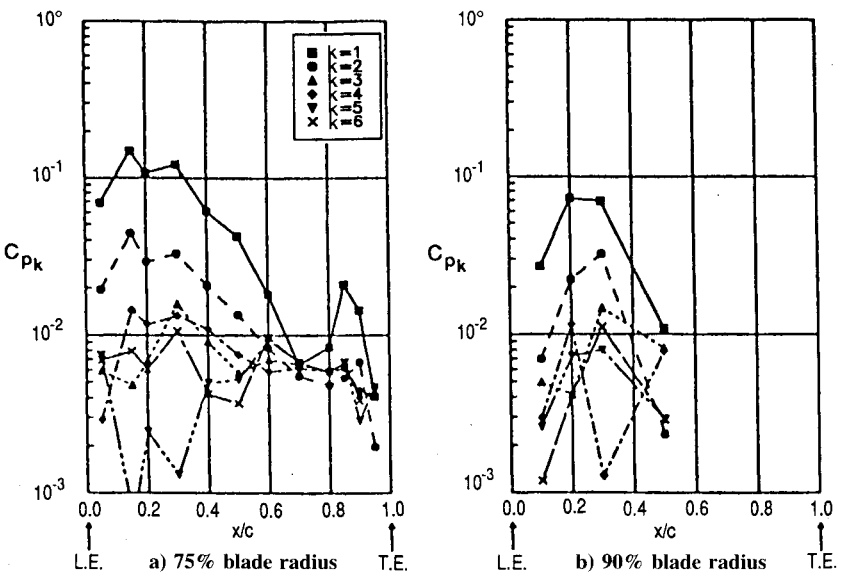

Fig. 2 Fourier analysis of unsteady pressure in flight condition 2.

Table 1 Summary of flight conditions

Condition	Altitude, ft	Indicated airspeed, kt	rpm	Flap, deg	M_r 0.75R	M_r 0.90R	$\Delta\beta$, deg 0.75R	$\Delta\beta$, deg 0.9R	J
2	35,000	120	1,700	0	0.687	0.788	4.3	2.7	1.47
4	35,000	150	1,700	0	0.754	0.848	3.8	2.7	1.91
11	15,000	120	1,700	0	0.85	0.682	0.9	0.3	1.13
18	15,000	150	1,700	20	0.598	0.693	3.3	1.4	1.27
24	15,000	150	2,000	35	0.687	0.799	3.2	1.0	1.15

For the spectral methodology applied to a digitized time series, similar to our problem, Refs. 6–8 may be consulted. From Eq. (2), a nondimensional, unsteady surface pressure coefficient is defined as

$$C_{P_k} \equiv (P_k)_{\text{rms}}/[(\gamma/2)P_\infty M_r^2] \tag{3}$$

where $\gamma/2P_\infty M_r^2$ is the relative-to-propeller dynamic pressure.

Chordwise evolution of the harmonic decomposition of unsteady surface pressure is shown in Fig. 2 for flight condition 2. Summary of flight conditions and important propeller flow parameters are listed in Table 1. Small rms amplitudes of higher harmonics (e.g., $n \geq 3$) has prompted the use of logarithmic scale in Fig. 2. At the 75% propeller radius (Fig. 2a), the first three harmonics ($k = 1, 2, 3$) exhibit similar initial growth and subsequent decay characteristics. Higher harmonics ($k = 4, 5, 6$) show small-amplitude random oscillations. At about 70% chord ($x/c \cong 0.7$), fundamental and all higher harmonics converge to a common value of C_{pk} (nearly 6×10^{-3}). This point is therefore called a random pressure fluctuation node, where all harmonics exhibit the same Fourier amplitude. The significance of the existence of the node, its location, and influence on the near-field radiated noise pattern are of interest to acoustic modeling of pusher propellers, and are under investigation. The trailing-edge footprint of the rapid fundamental wave growth to a local maximum at $x/c = 0.85$ is interpreted as unsteady vortex shedding. Higher harmonics in the Fourier analysis do not show significant amplitudes near the trailing edge.

Fourier decomposition of the unsteady surface pressure at the instrumented propeller 90% radius is shown in Fig. 2b. Only four pressure transducers on the suction surface at $x/c = 0.1$, 0.2, 0.3, and 0.5 were operational in flight condition 2. Fundamental and $k = 2$ harmonics exhibit similar trends in growth and decay characteristics. However, the rms amplitude of the fundamental wave is nearly five times larger than the first harmonic. The rms amplitudes of $k = 3$, 4, 5, and 6 modes are all small and exhibit random behavior. To examine the trailing-edge response of the 90% propeller radius to incoming flow nonuniformities (e.g., upstream wake interaction) requires BMTs beyond 80% chord. This was not foreseen prior to flight testing and data reduction; hence, the unsteady trailing-edge behavior (at 0.9R) is totally unavailable in our investigation. We anticipate, however, a response at 0.9R qualitatively similar to that obtained at 0.75R propeller section. A comparison between the working BMTs at 0.9R and their counterparts at 0.75R reveals a lower amplitude pressure fluctuation at the tip. Lighter mean loading of the propeller near the tip and smaller incidence variation due to wake chopping are deemed responsible for this behavior (Table 1).

Flight condition 4 represents a higher helical Mach number and propeller advance ratio than flight condition 2 due to a higher flight speed. The spectral analysis of unsteady surface pressure for this flight condition is shown in Fig. 3. The chordwise growth and decay characteristics of these Fourier components of the unsteady disturbances are similar to those of flight condition 2 (Fig. 2). However, due to lighter loading of flight condition 4 as compared to 2, the rms amplitude of fundamental wave grows to a lower fraction of relative dynamic pressure than C_{P_1} in flight condition 2. The peak in C_{P_1} at 0.75R for flight condition 4 is 0.08, while it attains the value of 0.15 for condition 2. This difference in the fundamental wave growth in the two flight conditions points to the significance of blade loading in the radiated noise intensity of pusher propellers operating in the wake of a pylon, a wing, or an upstream blade row. The trailing-edge signature of a one-per-rev vortex shedding, due to pylon wake encounter, is also interpreted from Fig. 3 with a local maximum in C_{P_1}

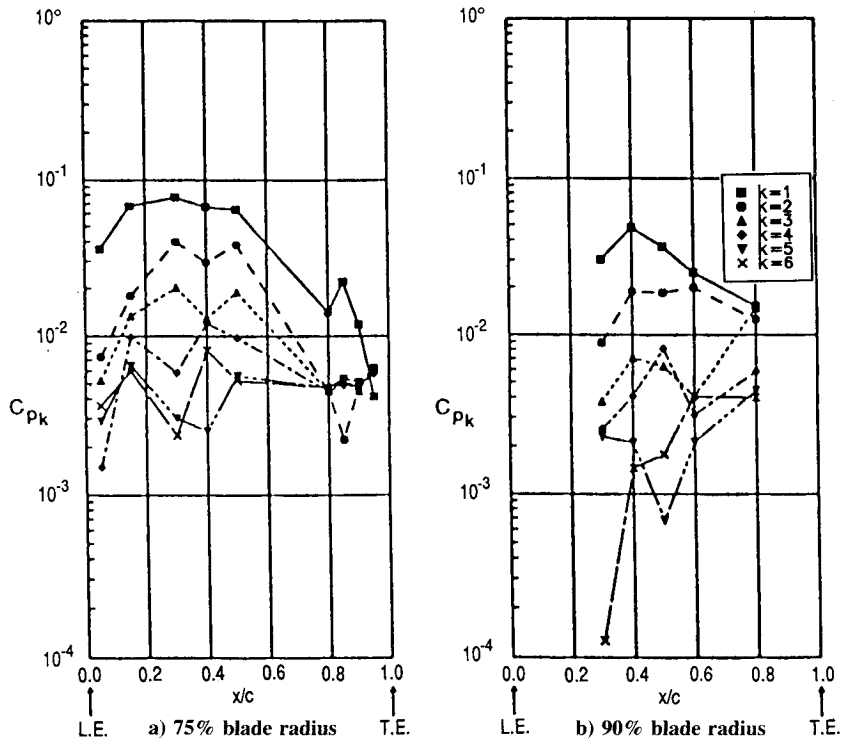

Fig. 3 Fourier analysis of unsteady surface pressure in flight condition 4.

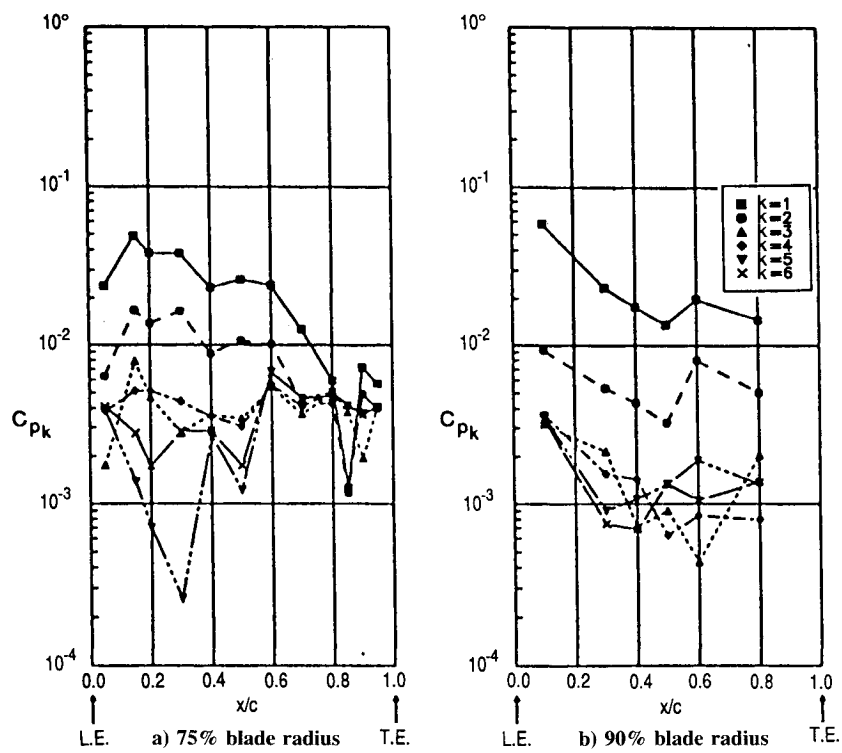

Fig. 4 Fourier analysis of unsteady surface pressure in flight condition 11.

at $x/c = 0.85$ for $0.75R$ propeller section. The peak in C_{P_1} near trailing edge is 0.02 for both flight conditions. Higher harmonics (i.e., $k = 2$–6 waves) behave similarly in flight conditions 4 and 2. The random pressure fluctuation node in Fig. 2a is located at 80% chord, where all Fourier components of the disturbance converge to a common rms amplitude, except the fundamental wave. Fluctuations at $0.9R$ propeller section in flight condition 4 (shown in Fig. 3b), in general, attain lower rms levels than $0.75R$ propeller section, and do not exhibit the same peak levels attained on the propeller tip section in flight condition 2.

Spectral analysis of unsteady surface pressure in flight condition 11 is shown in Fig. 4. This flight condition represents the lowest flight speed and propeller loading among all the flight conditions tested (Table 1). The dominating fundamental wave evolves similarly along the propeller chord, as in the cases discussed earlier. The rms peak level attained at 15% chord for the three-quarter propeller section is 0.05, which is lower than the previous cases. Interestingly, a fluctuating pressure node at 80% chord appears in this flight condition for the $0.75R$ propeller section as well. Furthermore, a lower-intensity, unsteady vortex shedding phenom-

enon is interpreted from frequency-domain data in this flight condition, as shown in Fig. 4a. In addition, both fundamental and first harmonic (i.e., C_{P_1} and C_{P_2}) exhibit local maxima at 90% chord, which suggest at least two unsteady vortex sheddings per revolution at the propeller trailing edge in this flight condition. In the earlier cases (i.e., conditions 2 and 4) the first harmonic did not exhibit a local maximum of large amplitude near the trailing edge. At the tip section, Fig. 4b, the fundamental wave shows a peak rms value comparable to the $0.75R$ section with the first harmonic, $k = 2$, copying the fundamental trend with nearly a factor of five smaller rms amplitude. All higher harmonics ($k = 3$, 4, 5, and 6) decay to a random turbulence level along the chord.

Due to close coupling of the aft fuselage-mounted pusher propeller and the wing on the testbed aircraft, a series of flight tests with various degrees of positive flap deflection were conducted.[1] Among these, flight conditions 18 and 24 were selected for their high propeller mean loading conditions, as well as a large number of operating BMTs in both flight conditions. A pressure rake survey of pylon wake in flight indicated a much wider wake—i.e., with nearly 2–3 times the width—when positive flap deflections of 20 and 35 deg were applied.[1] This pointed to a possible flow separation from the pylon, and that the propeller interacted with a more turbulent, wider upstream wake. Chordwise evolution of the Fourier decomposition of the unsteady surface pressure is shown in Figs. 5 and 6 for flight conditions 18 and 24, respectively. The interesting and distinctive feature of the Fourier components in these flight conditions is seen at the trailing edge (in Figs. 5 and 6), for the $75R$ propeller section, which are interpreted as a multiple vortex shedding phenomenon. This behavior was absent in other flight conditions investigated so far. It must be noted that periodic or multiple vortex shedding phenomena had earlier been observed in axial-flow compressor stages. The propeller tip response to upstream distortion (Figs. 5b and 6b) is dominated, as before, by the upstream wake encounter with the first harmonic, $k = 2$, following the trend with 5–10 times smaller rms amplitude. All higher harmonics fall off to very small amplitudes, i.e., to levels corresponding to boundary-layer random turbulence.

Performing joint statistical calculations on selected transducers' signals leads to a better physical understanding of the dynamical system under investigation. The pusher propeller flowfield, in our problem, forced by a highly localized (roughly

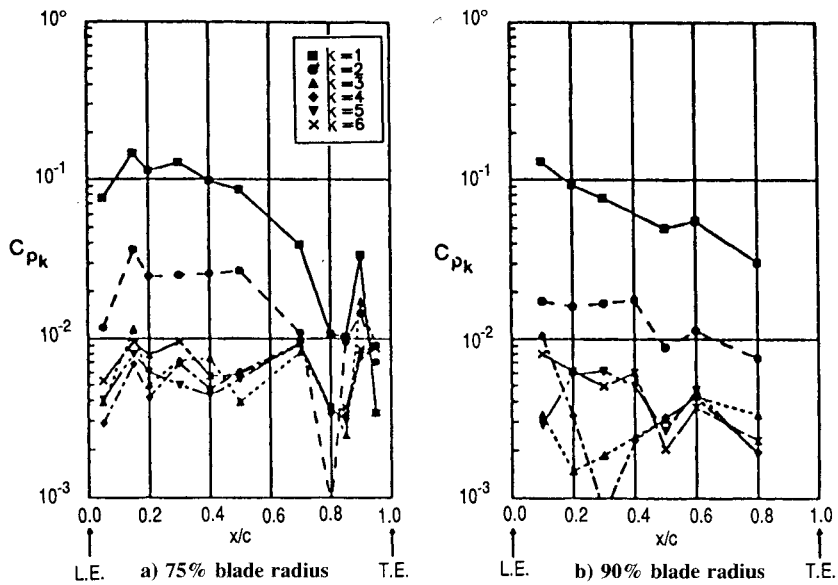

Fig. 5 Fourier analysis of unsteady surface pressure in flight condition 18.

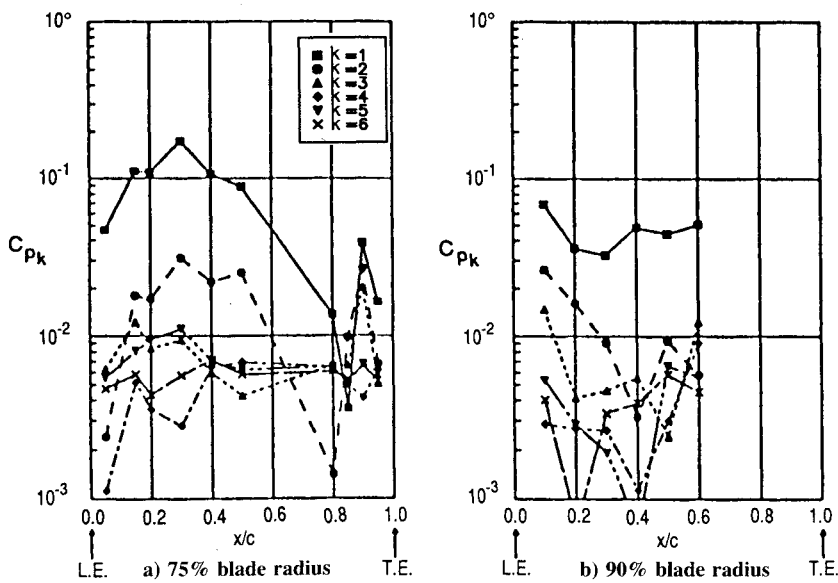

Fig. 6 Fourier analysis of unsteady surface pressure in flight condition 24.

of 10-deg azimuthal extent), one-per-rev, periodic disturbance (i.e., the upstream wake) comprises the dynamic system. The propeller flowfield response to pylon wake, based on flight data analysis, is primarily dominated by a leading-edge vortex separation and a trailing-edge vortex-shedding phenomenon. Hence, the blade-mounted transducers where the fundamental wave achieves its maximum, near leading and trailing edges, are selected for joint statistical analysis. In particular, we are interested in the question of linearity or nonlinearity of the frequency response behavior of the vortex formation and shedding on a pusher propeller interacting with a single upstream wake per revolution. For this purpose, coherence function $\gamma^2_{\xi,\eta}(f)$ is calculated using

$$\gamma^2_{\xi,\eta}(f) = \frac{|G_{\xi\eta}(f)|^2}{G_{\xi\xi}(f)G_{\eta\eta}(f)} \tag{4}$$

where ξ and η are BMT digitized time signals on two different points on the propeller suction surface at $0.75R$ section; also $G_{\xi\eta}(f)$ is defined as

$$G_{\xi\eta}(f) = (2/T)E[\xi^*_T(f)\eta^*_T(f)] \tag{5}$$

where $\xi^*_T(f)$ and $\eta^*_T(f)$ are complex conjugates of finite Fourier transform of sample record $\xi(t)$ and finite Fourier transform of $\eta(t)$, respectively, over a period of T. Furthermore, $G_{\xi\xi}(f)$ and $G_{\eta\eta}(f)$ are power-spectral densities of BMT digitized time series $\xi(t)$ and $\eta(t)$, respectively, and are defined as

$$G_{\xi\xi}(f) = (2/T)E[|\xi_T(f)|^2] \tag{6}$$

$$G_{\eta\eta}(f) = (2/T)E[|\eta_T(f)|^2] \tag{7}$$

To arrive at close estimates of finite Fourier transforms of sample records $\xi(t)$ and $\eta(t)$—i.e., $\xi_T(f)$ and $\eta_T(f)$—we have utilized fast Fourier transform (FFT) techniques detailed in Refs. 8–10.

In flight condition 2, the $\xi(t)$ and $\eta(t)$ are chosen at 15 and 85% chordwise locations, where the fundamental wave has grown to a local maximum (Fig. 2a). The coherence function between these transducers is shown in Fig. 7. Taking values of coherence function between 0.9–1 to represent linear frequency response behavior, we note that the fundamental and first harmonic (i.e., $k = 2$) possess this character. This means that the leading-edge vortex formation and trailing-edge vortex shedding are tied in a linear relationship where a linear-frequency response function with proper gain and phase factors can now be established between them. According to classical unsteady aerodynamic theory, this represents an expected result. The same statement may be applied to the first harmonic, $k = 2$, of the periodic forcing. To consider values of coherence function between 0.8–0.9 as a weakly nonlinear frequency response behavior, we note that the third harmonic, $k = 4$, falls under this category. All harmonics

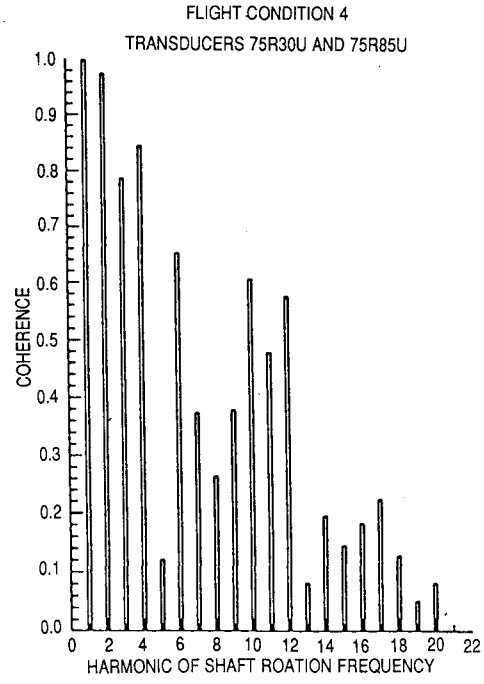

Fig. 8 Coherence function between 30- and 85%-chord BMT signals (flight condition 4).

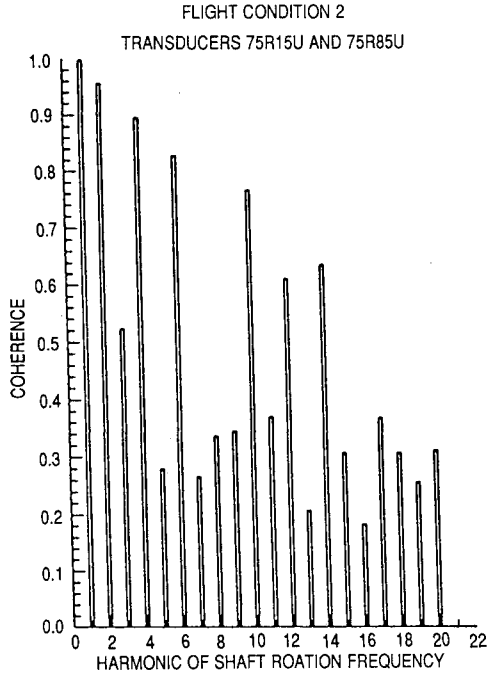

Fig. 7 Coherence function between 15- and 85%-chord BMT signals (flight condition 2).

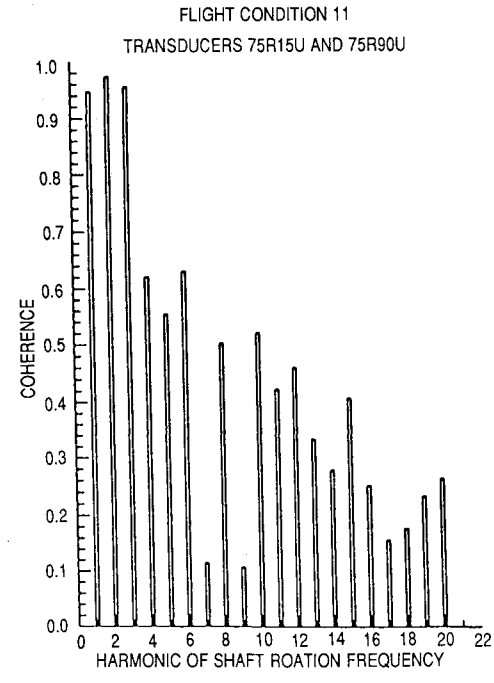

Fig. 9 Coherence function between 15- and 90%-chord BMT signals (flight condition 11).

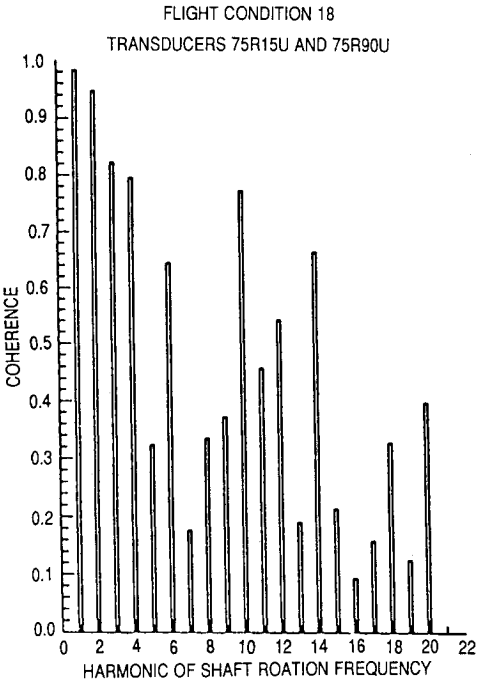

Fig. 10 Coherence function between 15 and 90%-chord BMT signals (flight condition 18).

with coherence function below 0.8 are then considered as having nonlinear behavior.

The coherence function between the 30- and 85%-chord BMT signals, in flight condition 4, is shown in Fig. 8. A very similar frequency response behavior is observed in this case as compared to flight condition 2. It is interesting to note that the coherence function between the fundamental waves at the transducers with maximum C_{P_1} growth, in both flights, is identically 1. This implies that a perfect linear relationship between leading- and trailing-edge vortex formation and shedding phenomena exists. Examining coherency in a lightly loaded propeller case (e.g., flight condition 11) reveals a value of 0.94 for the fundamental wave coherence function between transducers 15 and 90% chord (Fig. 9). The lack of perfect linearity between the leading-edge vortex separation and the trailing-edge vortex shedding may be traced to the weakness of these vortical structures in this lightly loaded case. First and second harmonics (i.e., $k = 2$ and 3) also possess linear frequency response character in flight condition 11. As a final case in this article, we consider coherence function in flight condition 18, where a positive 20-deg flap was applied. For this purpose, 15- and 90%-chord BMTs are chosen. Figure 10 shows the coherence function between these transducers. A value of 0.98 for the fundamental wave coherence function could suggest that this flight condition represents a higher propeller loading than condition 11, which, in light of Table 1, supports our earlier assertion. The first harmonic in this flight condition follows a linear frequency response behavior as in the earlier cases, while all higher harmonics exhibit a nonlinear spectral character. To develop linear frequency response function between leading- and trailing-edge large-scale coherent vortical structures on a pusher propeller is beyond the scope of this article. However, this is currently under investigation and will be reported in the future.

Concluding Remarks

Physical insight into unsteady aerodynamics and aeroacoustics of a rotating blade row operating in a distorted flow may be obtained by statistical analysis of unsteady surface pressure. Frequency-domain analysis of the fluctuating surface pressure reveals coherent and random contents of the flowfield under investigation. Periodic leading-edge vortex formation and trailing-edge vortex shedding are interpreted from our analysis and are believed to represent the main features of unsteady propeller interaction with an upstream wake. Joint statistical analysis reveals a linear frequency response character for the fundamental and first harmonic disturbances between selected BMTs on the propeller surface. Fourier components with higher frequencies behave nonlinearly in their joint spectral properties and represent random turbulence on the propeller blade surface unsteady flowfield. Further analyses, of flight data similar to this article, are needed to develop an analytical unsteady aerodynamic loading model to be used in propeller acoustic prediction codes.

Acknowledgments

Propeller-blade-surface unsteady pressure data in flight were obtained under NASA Langley Research Grant NAG-1-867. Feridon Farassat served as the technical monitor and has continued to provide valuable input to our work, for this, we are indebted to him.

References

[1]Farokhi, S., "Pressure-Time History of Pylon-Wake on a Pusher Propeller in Flight," *Journal of Propulsion and Power*, Vol. 6, No. 6, 1990, pp. 758–768.

[2]Farokhi, S., "Analysis of Flight Data Obtained on a Pusher Propeller on a Turboprop Testbed Aircraft: Volumes I–III," Univ. of Kansas Flight Research Lab. Rept. KU-FRL-803-2, Lawrence, KS, May 1990.

[3]Heidelberg, L. J., and Clark, B. J., "Preliminary Results of Unsteady Blade Surface Pressure Measurements for the SR-3 Propeller," AIAA Paper 86-1893, July 1986; see also NASA TM-87352, July 1986.

[4]Ditmar, J. H., and Jeracki, R. J., "Noise of the SR-3 Propeller Model at 2° and 4° Angle of Attack," NASA TM-82738, June 1981.

[5]Schoenster, J. A., "Fluctuating Pressure Measurements on the Fan Blades of a Turbofan Engine During Ground and Flight Tests," AIAA Paper 83-06079, April 1983.

[6]Hanson, D. B., "Study of Noise Sources in a Subsonic Fan Using Measured Blade Pressures and Acoustic Theory," NASA CR-2574, Aug. 1975.

[7]Bendat, J. S., and Piersol, A. G., *Random Data: Analysis and Measurement Procedures*, 2nd ed., Wiley-Interscience, New York, 1986.

[8]Bendat, J. S., and Piersol, A. G., *Engineering Applications of Correlation and Spectral Analysis*, Wiley-Interscience, New York, 1980.

[9]Brigham, E. O., *The Fast Fourier Transform*, Prentice-Hall, Englewood Cliffs, NJ, 1974.

[10]Oppenheim, A. V., and Shafer, R. W., *Digital Signal Processing*, Prentice-Hall, Englewood Cliffs, NJ, 1975.